Kinetic Modeling of Controlled Living Microemulsion Polymerizations That Use Reversible Addition–Fragmentation Chain Transfer

KEVIN D. HERMANSON,* SHIYONG LIU,† ERIC W. KALER

Center of Molecular Engineering and Thermodynamics, Department of Chemical Engineering, University of Delaware, Newark, Delaware 19716

Received 12 January 2006; accepted 23 June 2006
DOI: 10.1002/pola.21652
Published online in Wiley InterScience (www.interscience.wiley.com).

ABSTRACT: Reversible addition–fragmentation chain transfer (RAFT) polymerization is a useful technique for the formation of polymers with controlled architectures and molecular weights. However, when used in the polymerization of microemulsions, RAFT agents are only able to control the polymer molecular weight only at high RAFT concentrations. Here, a kinetic model describing RAFT microemulsion polymerizations is derived that predicts the reaction rates, molecular weight polydispersities, and particle size. The model predicts that at low RAFT concentrations, the RAFT agent will be consumed early in the reaction and that this will result in uncontrolled polymerization in particles nucleated late in the reaction. The higher molecular weight polydispersity that is observed in RAFT microemulsion polymerizations is the result of this uncontrolled polymerization. The model also predicts a shift in the conversion at which the maximum reaction rate occurs and a decrease in the particle size with increasing RAFT concentration. Both of these trends are also consistent with those observed experimentally. © 2006 Wiley Periodicals, Inc. J Polym Sci Part A: Polym Chem 44: 6055–6070, 2006

Keywords: controlled living polymerization; emulsion polymerization; microemulsion polymerization; kinetics (polym.); reversible addition fragmentation chain transfer (RAFT)

INTRODUCTION

In recent years, controlled living radical polymerization has become an important technique for the formation of polymers with controlled architectures and molecular weights.[1,2] One of the more important techniques for controlled free-radical polymerizations is reversible addition–fragmentation transfer (RAFT) polymerization. Although the RAFT process has been applied to numerous bulk and solution polymerizations, very few RAFT polymerizations have been successfully conducted in a heterogeneous polymerization environment.[3–5] Recently, a RAFT polymerization was successfully completed in a microemulsion.[6] In that case, 2-cyanoprop-2-yl dithiobenzoate (CPDB) was used in the polymerization of *n*-hexyl methacrylate (C_6MA), solubilized in a dodecyltrimethylammonium bromide (DTAB) microemulsion, yielding polymers with low polydispersities and low molecular weights for RAFT/initiator ratios above 3.0. At lower RAFT/initiator ratios, a shoulder developed in the

*Present address: E22-Biophysics, Department of Physics, Technische Universität München, 85747 Garching, Germany
†Present address: Department of Polymer Science and Engineering, University of Science and Technology of China, Hefei, 230026, Anhui Province, People's Republic of China
Correspondence to: E. W. Kaler (E-mail: kaler@che.udel.edu)

Journal of Polymer Science: Part A: Polymer Chemistry, Vol. 44, 6055–6070 (2006)

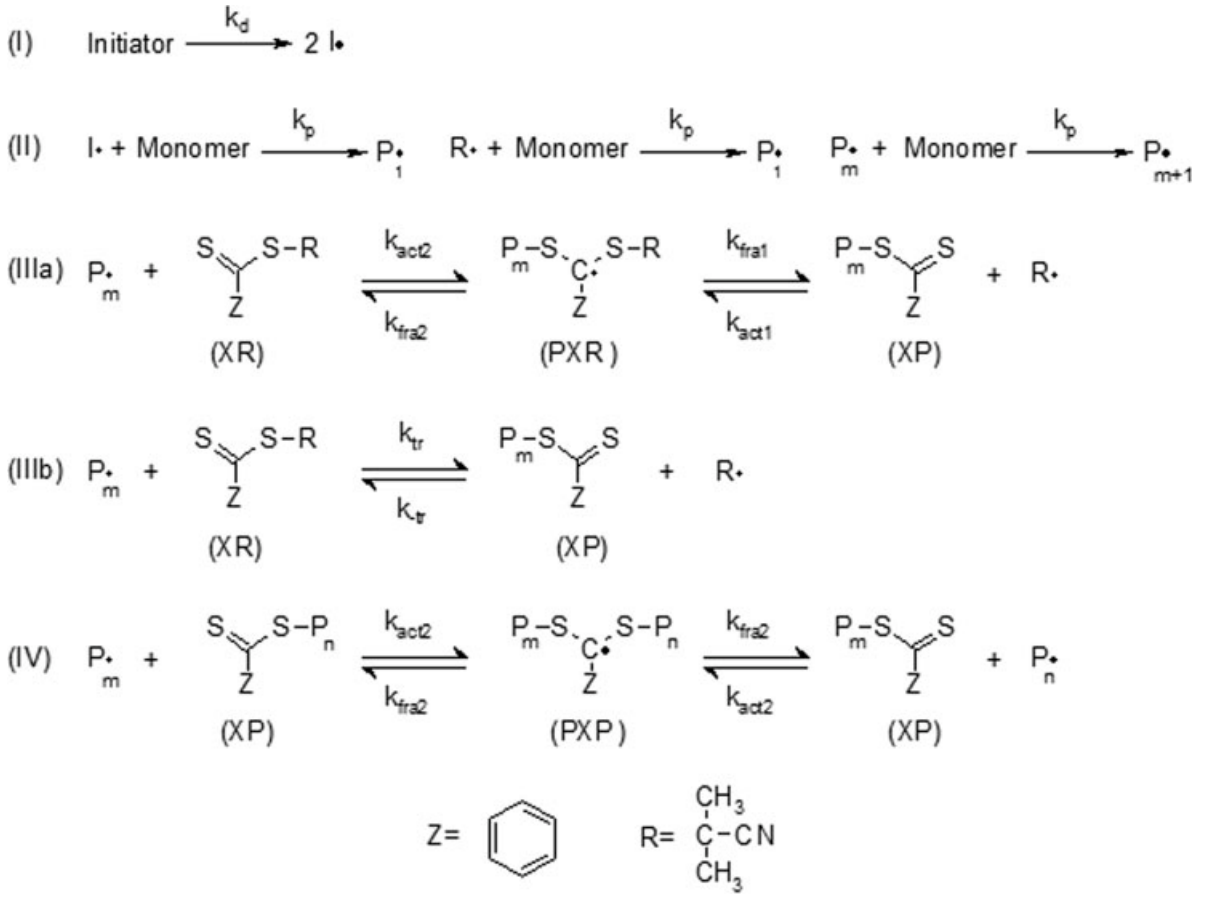

Scheme 1

final polymer molecular weight distribution, and this resulted in a high molecular weight polydispersity. An understanding of why this shoulder develops when RAFT is applied to microemulsion polymerizations would aid in the proper selection of RAFT agents for use in microemulsion formulations. To obtain a better understanding of the mechanisms leading to this unusual behavior, the polymerization kinetic model outlined here has been developed.

Kinetic models that describe the homogeneous RAFT process have previously been developed,[7–11] and some aspects of heterogeneous RAFT polymerizations have also been previously modeled.[12–16] Previous reports of kinetic modeling involve the use of rate constants that vary by as much as 7 orders of magnitude. The basis for these discordant rate constants is the unsettled debate over the inclusion of a combination termination mechanism.[7,17–27] Fortunately, in microemulsion polymerizations, there is not significant termination through combination,[28] so the polymerization mechanism is less ambiguous and the kinetics can be modeled with the mechanism shown in Scheme 1, which is similar to that used previously.[7]

The initiator molecules first decompose to give two initiator radicals (reaction I). The initiator radicals are then free to propagate with the monomer to form a polymer chain (reaction II). This polymer chain can either continue to react with the monomer or react with an unpolymerized RAFT agent (XR) to form a macro-RAFT radical (PXR; reaction IIIa). This macro-RAFT radical can then fragment to give either the initial polymer chain or a new initiator radical (R) and a polymerized RAFT agent (XP). If fragmentation results in an initiator radical, the newly formed initiator radical can react with the monomer to form a second polymer chain (reaction II). This second polymer chain will continue to propagate until it finds either an unpolymerized RAFT agent (XR) or polymerized RAFT agent (XP). If the second polymer chain finds a polymerized RAFT agent (XP), it can react to form the macro-RAFT radical (PXP; reaction IV). Once formed,

this macro-RAFT radical can fragment to give either of the attached polymer chains. Through reaction IV, an equilibrium is established between the active polymer chains (P) and the dormant polymer chains attached to the RAFT agent (XP). This equilibrium is the core mechanism and results in a reduced molecular weight polydispersity.

In this scheme, termination is assumed to occur at the same rate, regardless of the polymer chain size. As a result, all the macro-RAFT radicals are classified as either one of two species, PXR or PXP. PXR refers to a radical that contains both a polymer chain (P) and a cyanopropyl group (R), whereas PXP refers to a radical that contains two polymer chains. The reaction of a cyanopropyl radical with an unpolymerized RAFT agent is assumed to have a negligible effect on the kinetics. All radical species (R, I, and P) are assumed to propagate at the chain propagation rate (k_p). In this scheme, the value of rate constant $k_{fra,2}$ is controversial but is expected[7,18,20,22,27] to be within the very broad range of 10^{-2}–10^5 s^{-1}.

A common variation of Scheme 1 assumes a steady-state equilibrium for reaction IIIa. In this case, reaction IIIa becomes either an irreversible chain-transfer reaction with $k_{tr} = k_{act,2}k_{fra,1}/(k_{fra,2} + k_{fra,1})$ or a reversible chain-transfer reaction with both a forward rate constant, k_{tr}, and a reverse rate constant, $k_{-tr} = k_{act,1}k_{fra,2}/(k_{fra,2} + k_{fra,1})$ (reaction IIIb). For the microemulsion polymerization simulations reported here, the use of the steady-state assumption gave small but nonnegligible differences in the predicted results.

THEORY

Nonliving microemulsion polymerizations have been studied extensively, and a general mechanism by which they occur has been developed.[28–35] In a nonliving microemulsion polymerization, an initiator (typically water-soluble) is added to a one-phase and thermodynamically stable solution of monomer-swollen micelles. The added initiator first begins to propagate in the aqueous domain until a critical degree of polymerization is reached, whereupon the radical becomes sufficiently hydrophobic to enter a monomer-swollen micelle, thereby forming a polymer particle. Once entry has occurred, the radical continues to propagate until either it undergoes chain transfer to the monomer, by which exit may occur, or all the monomer in the microemulsion is consumed. The monomer consumed in the polymer particle by the radical is replenished by monomer diffusion from the uninitiated micelles. The concentration of the monomer at the locus of the polymerization is governed by thermodynamics.[28,33] Because there are a large number of micelles in comparison with the final number of particles, new particles are nucleated throughout the entire reaction, and biradical termination is negligible.

Kinetic Model for RAFT Polymerization

In the polymerization scheme used here, the initiator first decomposes in the aqueous domain to produce two radicals (reaction I in Scheme 1). The radical concentration in the aqueous phase is assumed to be in the steady state, and so the rate of radical entry (ρ) is equal to the rate of initiator decomposition:

$$\rho(t) = \gamma_{eff} 2k_d[\mathrm{I}] \exp(-k_d t) \quad (1)$$

where γ_{eff} is an efficiency constant that accounts for radical termination in the aqueous domain, k_d is the dissociation rate constant, [I] is the initiator concentration, and t is the time.

Once the initiator radical enters a monomer-swollen micelle, it begins to propagate and thereby forms a new polymer particle. The radical can react with either the monomer or the RAFT agent within the particle. It is assumed that the RAFT agent is free to exit a particle only if it has not yet reacted with a polymer chain (P_m). As a result, each polymerizing particle experiences a different local concentration of the RAFT agent, and subsequent reaction rates are then a function of both a given time (t) and the time at which the particle is initiated (t_1). On the basis of Scheme 1, the equations that describe the reaction rate within a particle initiated at time t_1 are

$$\frac{\partial PXR(t_1,t)}{\partial t} = k_{act,2} C_{XR}^{part}(t) P^*(t_1,t) + k_{act,1} C_{XP}(t_1,t) R^*(t_1,t) - (k_{fra,1} + k_{fra,2}) PXR(t_1,t) \quad (2)$$

$$\frac{\partial PXP(t_1,t)}{\partial t} = k_{act,2} C_{XP}(t_1,t) P^*(t_1,t) - 2k_{fra,2} PXP(t_1,t) \quad (3)$$

$$\frac{\partial C_{XP}(t_1,t)\phi_{part}(t_1,t)}{\partial t} = 2k_{fra,2}PXP(t_1,t) + k_{fra,1}PXR(t_1,t) - k_{act,1}C_{XP}(t_1,t)R(t_1,t) - k_{act,2}C_{XP}(t_1,t)P^*(t_1,t) \quad (4)$$

$$\frac{\partial R^*(t_1,t)}{\partial t} = -k_p R^*(t_1,t) C_{mon}^{part}(t) + k_{fra,1}PXR(t_1,t) - k_{act,1} C_{XP}(t_1,t)R^*(t_1,t) \quad (5)$$

$$\frac{\partial P^*(t_1,t)}{\partial t} = k_p R^*(t_1,t) C_{mon}^{part}(t) - k_{act,2} C_{XR}^{part}(t)P^*(t_1,t) - k_{act,2}C_{XP}(t_1,t)P^*(t_1,t) + 2k_{fra,2}PXP(t_1,t) + k_{fra,2}PXR(t_1,t) \quad (6)$$

where $R^*(t_1,t)$, $P^*(t_1,t)$, $PXP(t_1,t)$, and $PXR(t_1,t)$ are defined in Scheme 1 as radical concentrations per unit of volume of the microemulsion in a particle initiated between time t_1 and $t_1 + dt_1$; C_{XP} and C_{XR}^{part} are the concentrations of the macro-RAFT agent and unpolymerized RAFT agent per a unit of volume of the particle, respectively; C_{mon}^{part} is the concentration of the monomer in the polymer particle; and ϕ_{part} is the unit of volume of the polymerizing domain per unit of volume of the microemulsion.

When the size of the polymerizing domain is larger than a swollen micelle (ca. 3 nm), the volume of the polymerizing domain is equal to that of a monomer-swollen polymer chain of length L. $L(t_1,t)$ is the length of a chain initiated at time t_1 at a latter time t. L can be found from the average propagation rate of a radical. The average propagation rate is equal to the fraction of active particles multiplied by the propagation rate of those particles:

$$\frac{\partial L}{\partial t}(t_1,t) = k_p C_{mon}^{part}(t) \times \frac{P^*(t_1,t)+R^*(t_1,t)}{P^*(t_1,t)+R^*(t_1,t)+PXP(t_1,t)+PXR(t_1,t)} \quad (7)$$

The quotient on the right-hand side of eq 7 is the fraction of radicals initiated at t_1 that are still propagating at time t. The volume of a monomer-swollen polymer particle at time t is then given by

$$r(t_1,t) = \left(\frac{3MWL(t_1,t)}{4\pi\rho_{poly}N_A\left(1-\frac{C_{mon}^{part}(t)MW}{\rho_{mon}}\right)} \right)^{\frac{1}{3}} \quad (8)$$

and

$$\phi_{part}(t_1,t) = \frac{4}{3}\pi r(t_1,t)^3 N_A \rho(t_1) \quad (9)$$

where MW is the monomer molecular weight, N_A is Avogadro's number, ρ_{mon} is the bulk monomer density, and ρ_{poly} is the bulk polymer density.

At very small particle sizes, the volume of the polymerizing domain is dominated by the volume of the surfactant tails. In this case, the polymerizing domain resembles a micelle more than a polymer particle, and it is assumed that particles less than the size of the micelles (r = 3 nm)[36] have a radius equal to that of the monomer-swollen micelle.

C_{mon}^{part} and C_{XR}^{part} are not the same as the micellar concentrations because of thermodynamic partitioning. The partitioning of the monomer in nonliving polymerizations has been investigated previously for the same monomer and surfactant concentrations used in this study.[33] Those results show that the concentration at the reacting site decreases linearly with the polymer conversion. Thus

$$C_{mon}^{part}(t) = C_0(1 - f(t)) \quad (10)$$

where f is the monomer conversion and C_0 is the initial concentration of the monomer in the polymer particle. The partitioning of the unpolymerized RAFT agent (XR) is not known, but approximate values can be estimated under the assumption that the agent partitions similarly to the monomer (see the appendix). Equations 2–6 assume that the initiator-derived radicals (I in Scheme 1) behave identically to the RAFT-agent-derived radicals (R^* in Scheme 1). A further assumption is that the initiator and polymer radicals react with the monomer at the same rate. It has been argued by some[37] that the inhibition period observed in some bulk RAFT polymerizations may be due to the slow reaction rate of the RAFT leaving group (R) with the monomer. However, 2-cyanopropyl is a highly reactive leaving group, and in polymerizations of methyl acrylate, the rate of its reaction with the methyl acrylate monomer is larger than that of a methyl acrylate radical.[38] This is also true for the case modeled here because 2-cyanopropyl reacts with methacrylates faster than acrylates,[39] and acrylate radicals react faster with the monomer than methacrylate.[40,41] Therefore, in the modeling of CPDB/methacrylate RAFT polymerizations, the initiation rate can safely be taken to equal the polymer/monomer propagation rate.

To solve this set of equations, the concentration of initiator radicals that enter a particle between time t_1 and $t_1 + dt_1$ must be known. In

the case of no radical exit, this concentration is equal to the rate of initiator decomposition:

$$R^*(t_1,t) = \rho \text{ at } t = t_1 \tag{11}$$

The concentrations found by the solution of eqs 2–6 are thus for the particles initiated at times between t_1 and $t_1 + dt_1$, and the total concentration of each species can be found by summation over all t_1 values. The rate of monomer consumption is calculated by the multiplication of the total number of propagating radicals by the radical propagation rate:

$$\frac{\partial f_{\text{mon}}}{\partial t} = \frac{k_p\, C_{\text{mon}}^{\text{part}}(t)}{M_0} \int_0^t (R^*(t_1,t) + P^*(t_1,t))dt_1 \tag{12}$$

Similarly, the rate of unpolymerized RAFT agent (XR) consumption is given by

$$\frac{\partial f_{\text{XR}}}{\partial t} = \frac{1}{XR_0} \int_0^t (k_{\text{act},2}\, C_{\text{XR}}^{\text{part}}(t) P^*(t_1,t) - k_{\text{fra},2} PXR(t_1,t))dt_1 \tag{13}$$

where f_{mon} and f_{XR} are the conversions of the monomer and RAFT agent, respectively, and M_0 and XR_0 are the concentrations at the start of the reaction of the monomer and RAFT agent per liter of the microemulsion, respectively.

The predicted reaction kinetics of a RAFT microemulsion polymerization are given by the simultaneous solutions of eq A5 and eqs 1–13. With the method of moments, a similar set of equations can be derived that describes the evolution of the molecular weight and polydispersity (see the appendix). The discrete particle size distribution can be determined by the solution of eqs 1, 7 and 8 for all t_1 values and by the counting of the number of particles between size r and larger size $r + \Delta r$. The limit of this distribution as Δr approaches 0 yields the distribution $n_r(r, t)$, where $n_r(r, t)dr$ is the number of particles with a size between r and $r + dr$. The predicted z-average size that would be measured by quasielastic light scattering (QLS), neglecting the effect of the particle form factor, is

$$\langle r(t)\rangle_{\text{QLS}} = \frac{\int_0^\infty r^6 n_r(r,t)dr}{\int_0^\infty r^5 n_r(r,t)dr} \tag{14}$$

This kinetic model addresses two issues that are not a concern in nonliving microemulsion polymerization. First, because of the compartmentalization in microemulsion polymerizations, each RAFT agent is not accessible to each polymerizing radical. Once a macro-RAFT agent (XP in Scheme 1) reaches a critical degree of hydrophobicity, it is no longer able to exit the particle, and this situation results in a local polymer environment that is different from the average polymer environment. Therefore, the polymerization rate within a particle not only is a function of the overall time of reaction but also depends on the time at which the particle is nucleated. Here for simplification we assume that the critical degree of polymerization that inhibits the exit of a macro-RAFT agent or radical (XP, PXR, or PXP) is equal to 1 ($P_n = P_1$). Second, the concentration of the unpolymerized RAFT agent (XR in Scheme 1) in the particle will not equal the concentration in the surrounding micelles. The concentration will either be controlled by mass transfer (diffusion) from surrounding micelles or be set by a thermodynamic partition coefficient. Because CPDB has a solubility (0.12 mM)[6] close to that of C_6MA (0.4 mM)[35] and because the diffusion rate of C_6MA is high enough to enable thermodynamic partitioning,[28,33] it is assumed that the CPDB concentration in the particle will also be set by a partitioning coefficient, as discussed further in the appendix.

In this model, the small amount of the RAFT agent soluble in the aqueous domain is assumed to have a negligible effect on the initiation efficiency. The effect of the RAFT agent on initiation has been investigated with a modified Maxwell–Morrison model proposed by Smulders et al.[15] that assumes that reaction III in Scheme 1 can be modeled with only the irreversible chain-transfer constant, $k_{\text{tr}} = k_{\text{act},2}k_{\text{fra},1}/(k_{\text{fra},2} + k_{\text{fra},1})$. Using values for the polymerization studied here in the proposed Maxwell–Morrison equations, we have found that CPDB is predicted to have a negligible impact on the initiation efficiency for polymerizations in which the initial local micelle RAFT concentrations are less than 0.2 mM and k_{tr}/k_p is less than 1000.

This model also assumes that radical exit does not affect the polymerization kinetics. The exits of both cyanopropyl radicals and monomeric radicals produced by chain-transfer were initially included in the model. Preliminarily results showed that radical exit had a negligible effect on the polymerization kinetics, molecular weight, and particle size. The inclusion of the radical exit terms also often leads to numerical

instabilities, so they were omitted for the final calculations.

SOLUTION METHOD

We solved equations A5 and 1–13 by first assuming monomer and RAFT concentrations for time Δt. As an initial guess, the monomer and RAFT concentrations were assumed to decrease linearly from time zero to time Δt. With these assumed monomer and unpolymerized RAFT concentrations, eqs 1–9 and 11 were then solved for all t_1 values between time zero and Δt with the Fortran subroutine DDASSL.[42] The resulting species concentrations at time Δt were then known for all particle initiation times (t_1). The total concentrations of P^*, R^*, and PXR at Δt were found by integration over all t_1 values. With these total concentrations, and under the assumption of a linear change in the total concentration from time zero to Δt, new monomer and unpolymerized RAFT concentrations, $C_{\text{mon}}^{\text{part}}(t)$ and $C_{\text{RAFT}}^{\text{part}}(t)$, were determined by the solution of eqs 12, 13, and A5. If these newly calculated monomer and unpolymerized RAFT concentrations were not equal to the initially assumed concentrations, the new monomer and unpolymerized RAFT concentrations were then used as the assumed concentrations, and eqs 1–9 and 11 were once again solved. These steps were repeated until the assumed and calculated concentrations were equal. This process was repeated for subsequent time steps (Δt) until a time was reached at which the polymerization was near completion. A step size of $\Delta t = 2$ s or less yielded accurate numerical solutions.

RESULTS AND DISCUSSION

Figures 1 and 2(a,b) show the predicted reaction kinetics with appropriate values for the RAFT microemulsion polymerization of C_6MA under the experimental conditions used by Liu et al.[6] The propagation rate constant was approximated to be $k_p = 1500$ M^{-1} s^{-1} by the interpolation of pulsed-laser polymerization data for other linear alkyl methacrylates.[41] k_d of the initiator, V50, was used as supplied by the manufacturer ($k_d = 2.03 \times 10^{-4}$ s^{-1}), and γ_{eff} was assumed to be 0.25. The initial concentration of the monomer in the polymer particle, C_0, was found through the

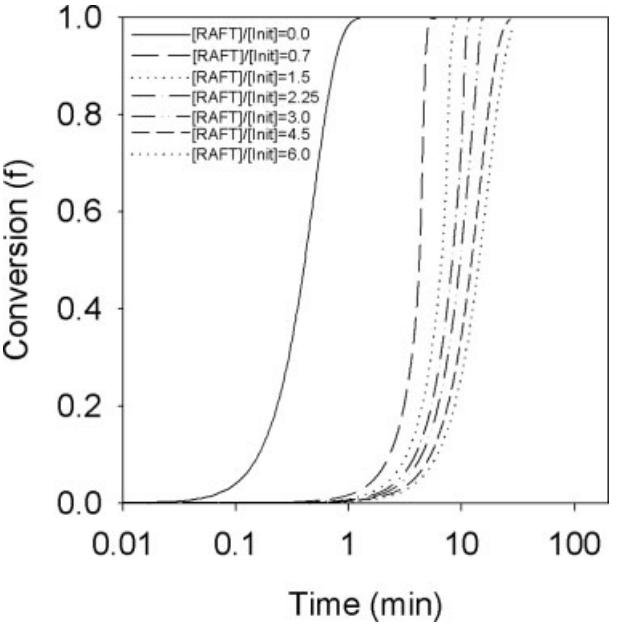

Figure 1. Model-predicted reaction kinetics at seven different RAFT concentrations with the following parameter values: $M_0 = 0.183$ M, [I] $= 6.1 \times 10^{-4}$ M, $C_0 = 4.5$ M, $\gamma_{\text{eff}} = 0.25$, $k_d = 2.03 \times 10^{-4}$ s^{-1}, $k_p = 1500$ M^{-1} s^{-1}, $k_{\text{fra},1} = 2.9$ s^{-1}, $k_{\text{fra},2} = 30$ s^{-1}, $k_{\text{act},1} = 7.5 \times 10^5$ M^{-1} s^{-1}, and $k_{\text{act},2} = 4.2 \times 10^5$ M^{-1} s^{-1}.

fitting of the Morgan–Kaler kinetic model,[28] which accurately describes the polymerization of DTAB/C_6MA/H_2O microemulsions, to kinetic data of polymerizations performed without a RAFT agent. The kinetic constants for the reaction of CPDB with C_6MA are unknown, but values for k_{act2}, k_{tr}, and $k_{-\text{tr}}$ have been measured for the polymerization of CPDB with methyl methacrylate.[43,44] For the purpose of these simulations, similar chain-transfer constants, $C_{\text{tr}} = k_{\text{tr}}/k_p$, $C_{-\text{tr}} = k_{-\text{tr}}/k_p$ (reaction IIIb Scheme 1), and $C_{\text{act},2} = k_{\text{act},2}/k_p$, were used as well as an assumed $k_{\text{fra},2}$ value of 30 s^{-1}. Values of $k_{\text{fra},2}$ in the range of 10^0–10^3 s^{-1} give kinetic rates of the appropriate order of magnitude and demonstrate similar kinetic trends. Figure 3 shows the effects of different $k_{\text{fra},2}$ values on the predicted kinetics for a [RAFT]/[Initiator] ratio of 1.5. Because few other simulations have been conducted on CPDB polymerized under either bulk or solution conditions, the accuracy of the $k_{\text{fra},2}$ value used is unknown. However, multiple simulations of styrene polymerizations with cumyl dithiobenzoate as the RAFT agent have been con-

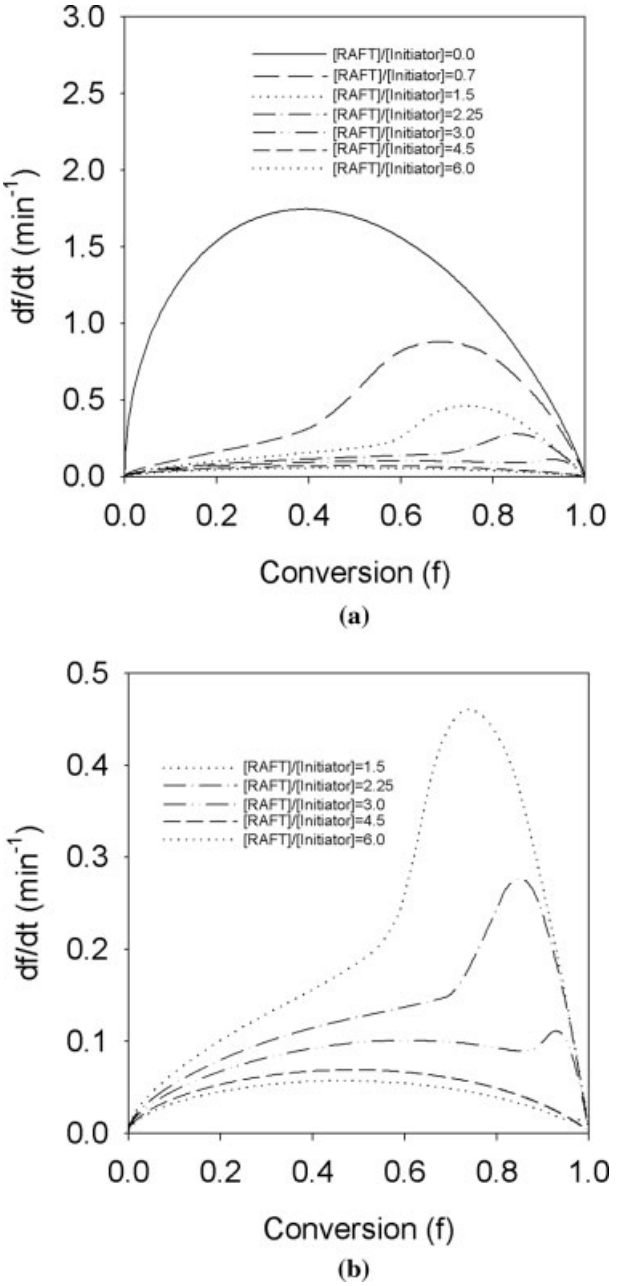

Figure 2. (a) Model-predicted reaction rates at seven different RAFT concentrations and (b) model-predicted reaction rates for five RAFT concentrations above [RAFT]/[Initiator] = 1.5 plotted with an expanded scale. For the parameter values, see Figure 1.

ducted[7,18,20–22] and have given values of $k_{fra,2}$ over the enormous range of 10^{-2}–10^{5} s^{-1}.

In accordance with the experimentally measured rates of Liu et al.[6] [Figs. 4 and 5(a,b)], the kinetics simulated here show a large decrease in the reaction rate with increasing RAFT concentrations [Figs. 1 and 2(a,b)]. However, the experimental kinetic rates could not be simulated quantitatively; this was most likely a result of the uncertainty in the values of the kinetic constants or because of constraints imposed by assumptions about the RAFT agent partitioning. In the simulated polymerizations, two kinetic rate intervals can be observed. In the first interval, the concentration of the unpolymerized RAFT agent available is high enough to mediate the polymerization effectively. As the polymerization progresses, the RAFT agent is consumed, and this results in a low concentration of the unpolymerized RAFT agent late in the reaction. As a result, newly nucleated particles can polymerize rapidly and without control. This situation causes the observed rapid increase in the reaction rate at higher conversions [Fig. 2(a,b)]. As the initial RAFT concentration increases, the length of the first interval is extended, and the amount of uncontrolled polymerization at the end of the reaction decreases.

When the RAFT concentration is high enough ([RAFT]/[Initiator] = 4.5 or 6.0), the RAFT agent is present throughout the entire reaction, and the full reaction proceeds under control. As a

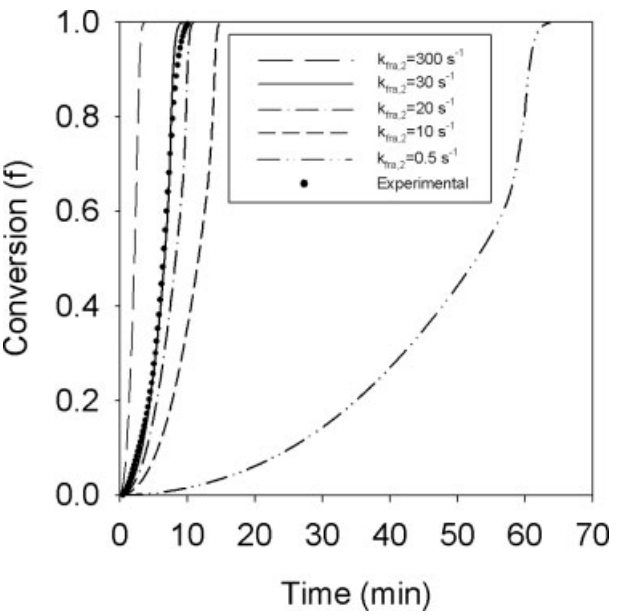

Figure 3. Model-predicted reaction kinetics at different $k_{fra,2}$ values for [RAFT]/[Initiator] = 1.5 with the following parameter values: M_0 = 0.183 M, [I] = 6.1 × 10^{-4} M, C_0 = 4.5 M, γ_{eff} = 0.25, k_d = 2.03 × 10^{-4} s^{-1}, k_p = 1500 M^{-1} s^{-1}, $k_{fra,1}$ = 2.9 s^{-1}, $k_{act,1}$ = 7.5 × 10^5 M^{-1} s^{-1}, and $k_{act,2}$ = 4.2 × 10^5 M^{-1} s^{-1}.

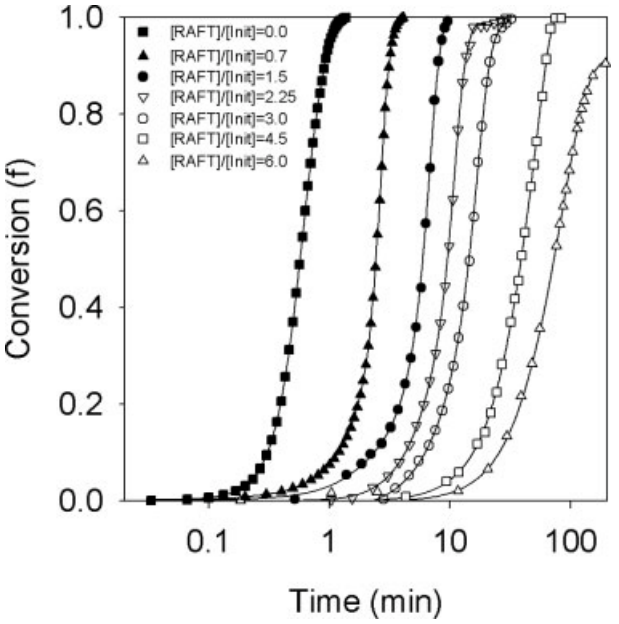

Figure 4. Experimentally measured reaction kinetics (cf. Fig. 1) at seven different RAFT concentrations (the experimental results were taken from ref. 6).

result, a shift in the maximum rate with increasing RAFT concentration is observed, and this is consistent with the shift observed in the experimental reaction rates [Fig. 5(a,b)]. When no RAFT agent is present, both the modeled and experimental reaction rate maxima occur at a conversion of 39% [Figs. 2(a) and 5(a)]. With the addition of the RAFT agent, the maximum rate shifts to higher conversions until a RAFT concentration is reached, at which the entire reaction is mediated by the RAFT agent. At the highest RAFT concentrations ([RAFT]/[Initiator] = 4.5 or 6.0), the maximum rate once again shifts to lower conversions [Figs. 2(a,b) and 5(a,b)].

The simulated trends in the final molecular weight polydispersity also resemble those measured[6] (Fig. 6). At low RAFT concentrations, the RAFT agent increases the molecular weight polydispersity. The experimental molecular weight distributions show that this increase results from the formation of a high-molecular-weight shoulder at low RAFT concentrations (Fig. 7). The simulation of these experiments shows that this increase in the polydispersity results from the early consumption of the RAFT agent and the subsequent uncontrolled polymerization. As the concentration of the RAFT agent increases, the effects of the RAFT agent become more beneficial, and beyond a critical concentration, the RAFT agent acts to decreases the polydispersity. The critical concentration is the concentration beyond which the unpolymerized

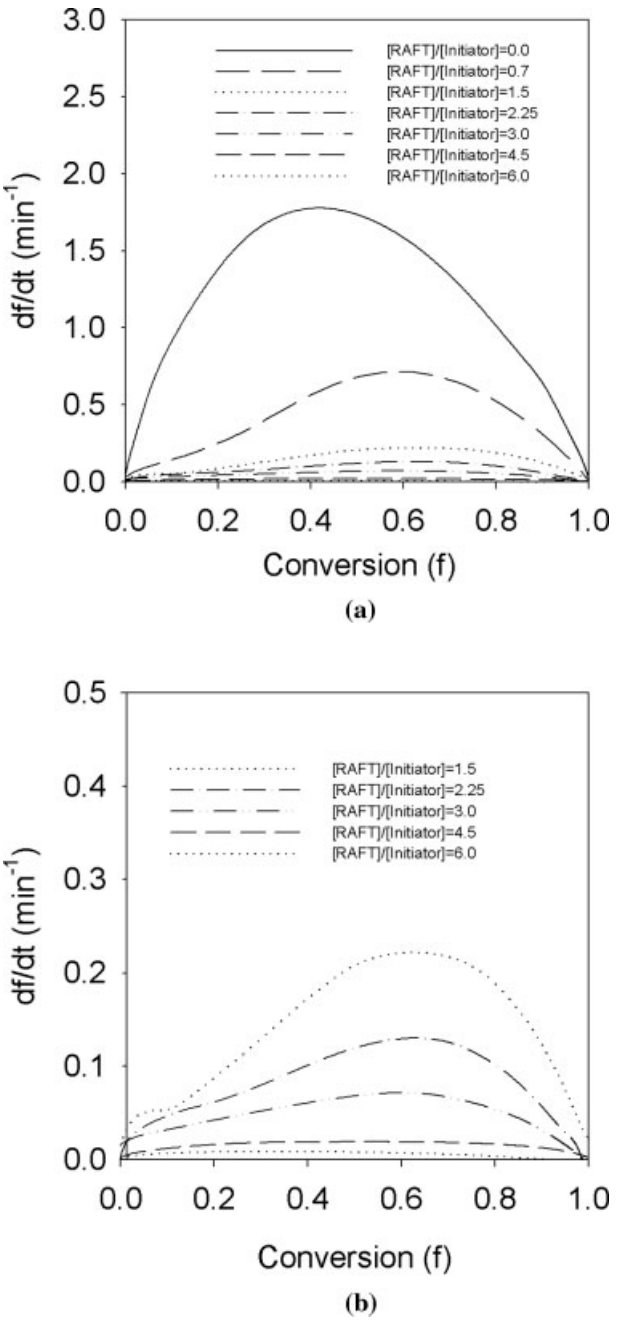

Figure 5. (a) Experimentally measured reaction rates [cf. Fig. 2(a)] at seven different RAFT concentrations and (b) experimentally measured reaction rates [cf. Fig. 2(b)] at five RAFT concentrations above [RAFT]/[Initiator] = 1.5 plotted with an expanded scale (the experimental results were taken from ref. 6).

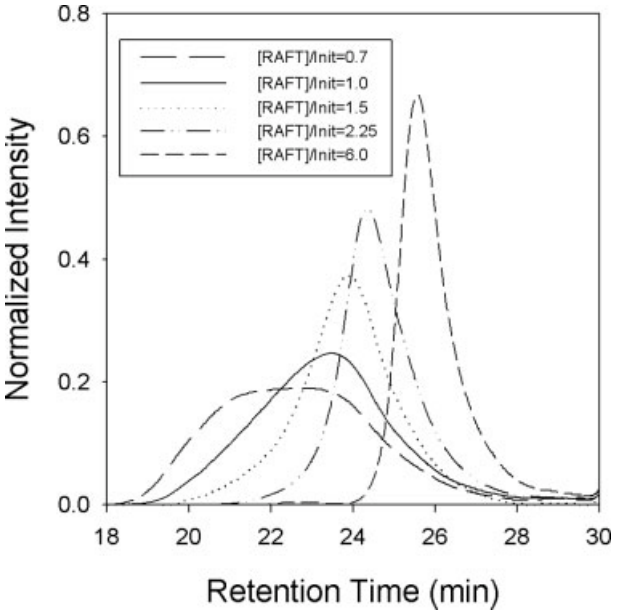

Figure 6. Gel permeation chromatography traces of final polymer samples at different RAFT concentrations. At low RAFT concentrations, a shoulder developed that corresponded to the formation of a high-molecular-weight polymer.

RAFT agent is present throughout the entire reaction, which is here equal to a [RAFT]/[Initiator] ratio slightly higher than 3.0.

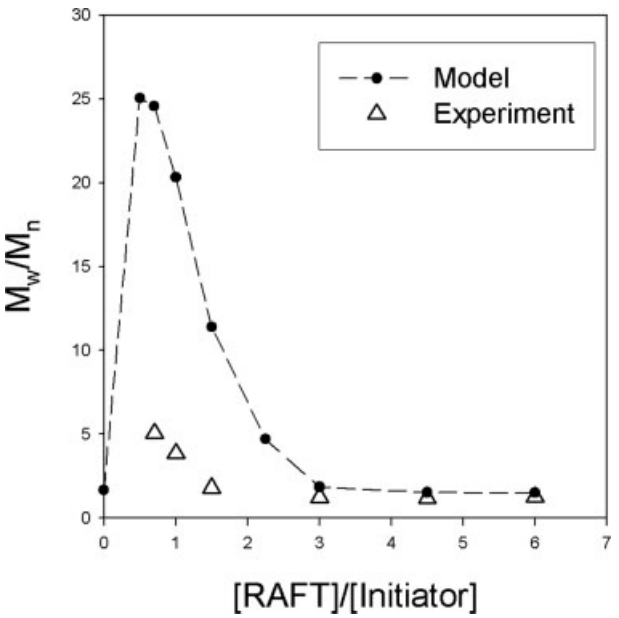

Figure 7. Effects of the RAFT concentration on the model-predicted polydispersities at 85% conversion and the final experimentally measured polydispersities (the experimental results were taken from ref. 6). For the parameter values, see Figure 1.

Figure 8 shows the simulated evolution of the molecular weight polydispersity. Early in the reactions, a low polydispersity is predicted at all RAFT concentrations, but late in the reaction, only the simulations at a high RAFT concentration predict a low polydispersity. Like the rapid increase in the polymerization rate observed at low RAFT concentrations and high conversions [Fig. 2(a,b)], the rapid increase in the polydispersity results from the early consumption of the RAFT agent and the uncontrolled polymerization of particles nucleated late in the reaction.

The critical RAFT concentration at which uncontrolled polymerization commences is determined by the consumption rate of the unpolymerized RAFT agent (III in Scheme 1). If the RAFT agent is consumed too quickly, the concentration of the unpolymerized RAFT agent decreases rapidly, and uncontrolled polymerization occurs late in the reaction. The rate of the RAFT agent consumption is determined by the kinetic rate k_{tr}. If this rate is too fast in comparison with the total reaction time, all the RAFT agent will be consumed too early in the reaction. In contrast, in bulk and solution polymerizations, there are no similar problems associated with the rapid consumption of the RAFT agent, although slow RAFT agent consumption and the resulting slow estab-

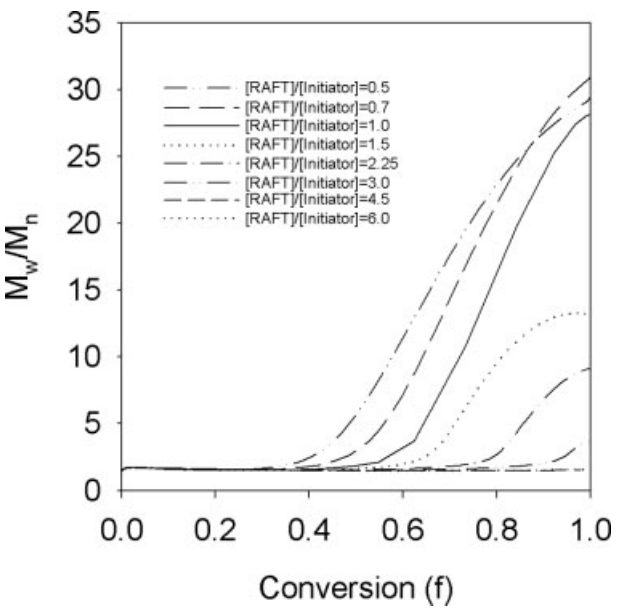

Figure 8. Model-predicted polydispersity as a function of the conversion at eight different RAFT concentrations. For the parameter values, see Figure 1.

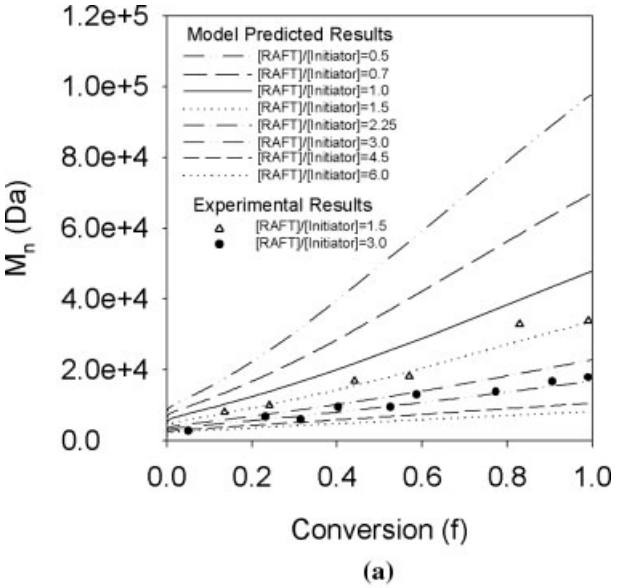

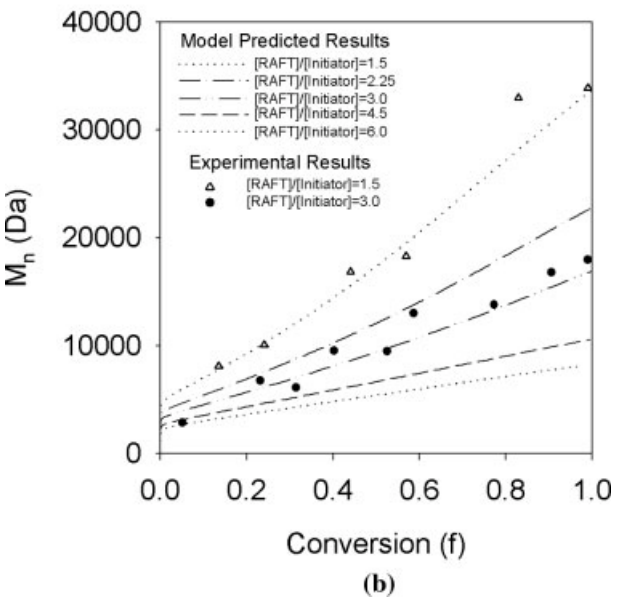

Figure 9. (a) Model-predicted and experimentally measured M_n as a function of the conversion at eight different RAFT concentrations and (b) model-predicted and experimentally measured M_n as a function of the conversion at five RAFT concentrations above [RAFT]/[Initiator] = 1.5 plotted with an expanded scale (the experimental results were taken from ref. 6). For the parameter values, see Figure 1.

lishment of equilibrium are often cited as causes for high molecular weight polydispersities.[2]

Even though the RAFT agent is continuously consumed throughout the polymerization, the simulated number-average molecular weight (M_n) increases linearly and agrees well with the experimentally measured molecular weight measured by Liu et al.[6] [Fig. 9(a,b)]. A linear increase in M_n is usually observed in bulk polymerizations[2] and results from RAFT agent consumption that is fast in comparison with the consumption of the monomer. If all the RAFT agent is consumed early in the reaction, M_n can be determined by the division of the total amount of the polymer formed by the total amount of the RAFT agent, and it is given by the following linear equation:

$$M_n = FW_{\mathrm{RAFT}} + \frac{M_0 FW_{\mathrm{mon}} f}{X R_0} \qquad (15)$$

where FW_{RAFT} and FW_{mon} are the RAFT and monomer molecular weights, respectively. Because the polymerization mechanism is much different in microemulsion polymerization, such linear behavior might be unexpected. The major difference between the M_n increase in microemulsion polymerization and that in solution and bulk polymerizations is that in microemulsion polymerization a line fit to the linear portion of the experimental data does not pass through the origin.

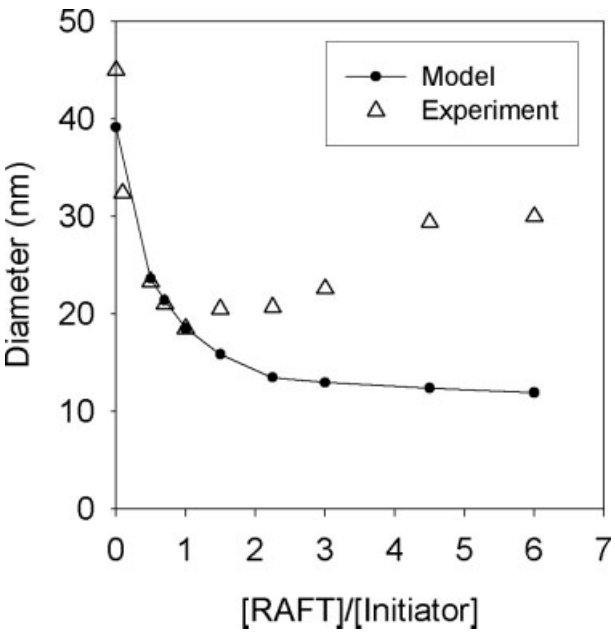

Figure 10. Effects of the RAFT concentration on the model-predicted particle size at 85% conversion, and the particle size experimentally measured by QLS (the experimental results were taken from ref. 6). For the parameter values, see Figure 1.

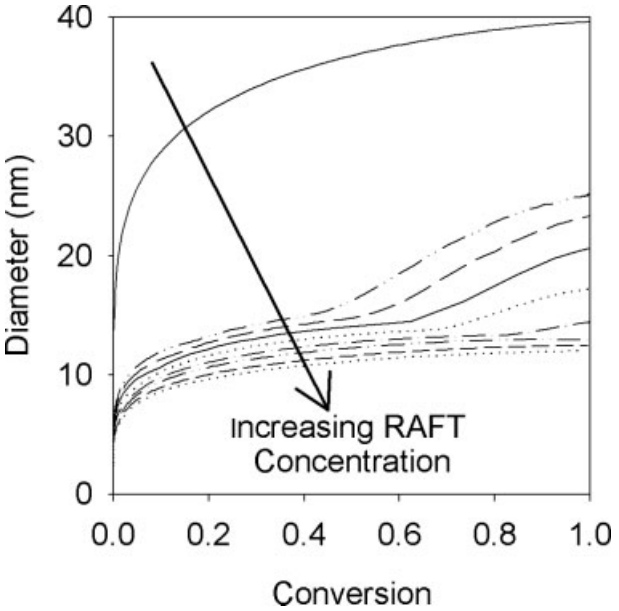

Figure 11. Model-predicted particle size as a function of the conversion at RAFT concentrations of 0, 0.5, 0.7, 1.0, 1.5, 2.25, 3.0, 4.5, and 6.0 ([RAFT]/[Initiator]). For the parameter values, see Figure 1.

The predicted particle size also shows a dramatic decrease with increasing RAFT concentration (Fig. 10) that is similar to the decrease observed experimentally.[6] However, unlike the experimentally measured particle size, at high RAFT concentrations, the simulated particle size continues to decrease. This difference between the experimental and simulated particle sizes is probably the result of particle aggregation and coagulation processes late in the reaction. These colloidal effects are not included in the model.

Figure 11 shows the simulated evolution of the particle size for different RAFT concentrations. At all RAFT concentrations, the simulated particle sizes are depressed in the initial stage of the reaction; however, for the low RAFT concentration simulations, the particle size increases rapidly at high conversions. The onset of this particle size increase corresponds to the onset of the uncontrolled polymerization, as observed in the polymerization kinetics [Fig. 2(a,b)].

CONCLUSIONS

The proposed model demonstrates that in polymerizations at low RAFT concentrations, the large molecular weight polydispersity, particle size, and reaction rates observed experimentally at high conversions likely result from the early consumption of the RAFT agent and the subsequent uncontrolled polymerization. The general trends predicted by the model mirror the experimental measurements, but uncertainties in the values of the kinetic parameters have prohibited quantitative predictions. Despite these limitations, the model is useful for the investigation of RAFT microemulsion polymerization mechanisms. The predicted kinetics also demonstrate a shift in the maximum rate that is consistent with that observed experimentally. The proper orders of magnitude in the particle size, molecular weight, and reaction rate have been obtained with $k_{fra,2}$ values in the range of 10^0–10^3.

The authors are grateful to D. G. Vlachos for his guidance in appropriate approaches to the numerical calculations herein.

APPENDIX

Raft Partitioning

The partitioning of a monomer or RAFT agent between polymer particles and swollen micelles can be written in terms of a thermodynamic partitioning constant (K):

$$K = \frac{C^{\text{part}}}{C^{\text{mic}}} \tag{A1}$$

where C^{part} is the monomer or RAFT concentration in the polymer particle and C^{mic} is the monomer or RAFT concentration in the micelles. Equation 10 can be written in terms of the monomer partitioning constant:

$$K_{\text{mon}}(t) = \frac{C_0}{C^{\text{mic}}_{\text{mon}}}(1 - f(t)) \tag{A2}$$

where K_{mon} is equal to $C^{\text{part}}_{\text{mon}}/C^{\text{mic}}_{\text{mon}}$. $C^{\text{mic}}_{\text{mon}}$ is the molar density of the monomer in the micelles:

$$C^{\text{mic}}_{\text{mon}} = \frac{(1-f)M_0 - \frac{C^{\text{part}}_{\text{mon}} f M_0 MW}{\rho_{\text{poly}}\left(1 - \frac{C^{\text{part}}_{\text{mon}} MW}{\rho_{\text{mon}}}\right)}}{\left(\frac{(1-f)M_0 MW}{\rho_{\text{mon}}} - \frac{C^{\text{part}}_{\text{mon}} f M_0 MW^2}{\rho_{\text{mon}}\rho_{\text{poly}}\left(1 - \frac{C^{\text{part}}_{\text{mon}} MW}{\rho_{\text{mon}}}\right)} + \phi_{\text{surf}}\right)} \tag{A3}$$

ϕ_{surf} is the volume fraction of the surfactant in the microemulsion.

Assuming the unpolymerized RAFT agent behaves in away thermodynamically similar to the monomer [$K_{mon}(t) = K_{RAFT}(t)$], the RAFT partitioning can be described by

$$K_{RAFT}(t) = \frac{C_0}{C_{mon}^{mic}}(1 - f(t)) \tag{A4}$$

Combined with the RAFT mass balance and under the assumption that the RAFT agent contributes a negligible volume to both the particle and micelles, the concentration of the unpolymerized RAFT agent in the polymer particle is

$$C_{XR}^{part} = \frac{K_{RAFT}(1 - f_{XR})XR_0}{\left[\frac{(1-f)M_0}{\rho_{mon}} - \frac{C_{mon}^{part} f M_0 MW}{\rho_{mon}\rho_{poly}\left(1 - \frac{C_{mon}^{part} MW}{\rho_{mon}}\right)}\right] MW + \phi_{surf} + K_{RAFT}\left(\frac{f M_0 MW}{\rho_{poly}\left(1 - \frac{C_{mon}^{part} MW}{\rho_{mon}}\right)}\right)} \tag{A5}$$

Molecular Weight Model

Recently, Wang and Zhu[8] developed a polymerization model based on the method of moments that describes the evolution of the molecular weight and polydispersity of a bulk RAFT polymerization in which the macro-RAFT radicals, PXP and PXR, do not terminate through biradical combination. Because a microemulsion polymerization contains negligible amounts of biradical termination, the evolution of the molecular weight and polydispersity can be calculated in a similar way.

The method of moments is a discrete transformation method that allows for the first three moments of the molecular weight distribution to be determined without the calculation of the entire distribution. In the method of moments, a generating function transform is applied to the concentration-based kinetic rate equations, transforming these equations into a set of moment-based kinetic rate equations. A good review of the method of moments was published by Dotson et al.[45] Here, the method of moments is used to calculate the evolution of the molecular weight and polydispersity of a RAFT microemulsion polymerization.

The goal of this derivation is to determine the moments of the molecular weight distribution for the four types of chain species (P_r, C_{XPr}, P_rXP_0, and $\sum_{s=1}^{r-1} 1/2 P_{r-s}XP_s$). In the notation used in this derivation, subscript r denotes the chain length, and the summation over $P_{r-s}\mathrm{XP}_s$ gives the number of macro-RAFT radicals (PXP) of total chain length r. The unpolymerized cyanopropyl radicals, which are usually represented by R^*, are now represented by P_0 in this symbolism. Similarly, macro-RAFT radicals (PXR) are represented by P_rXP_0.

A generating function transform operator is applied to four species in the concentration-based rate equations to give a set of moment-based rate equations. For example, the transform operator $\mathbf{Y}_i \equiv \sum_{r=1}^{\infty} r^i$ will be used to transform P_r in the concentration-based rate equations to moment-based rate equations that are in terms of Y_i, where Y_i is defined as the ith moment of P_r:

$$Y_i = \sum_{r=1}^{\infty} r^i P_r \tag{A6}$$

The transformed rate equations for the first three moments (Y_1, Y_2, and Y_3) can then easily be solved. Similarly, transforms are also applied to species P_rXP_s, C_{XPr}, and P_rXP_0 in the concentration-based rate equations, giving moment-based rate equations with moments that are defined as follows:

$$G_i = \sum_{r=1}^{\infty} r^i C_{X\,Pr} \tag{A7}$$

$$H_i = \sum_{r=1}^{\infty} r^i P_r \mathrm{XP}_0 \tag{A8}$$

$$Q_i = \frac{1}{2}\sum_{r=1}^{\infty} r^i \sum_{s=1}^{r} P_{r-s}\ \mathrm{XP}_s - \frac{1}{2}\sum_{r=1}^{\infty} r^i P_r \mathrm{XP}_0 \tag{A9}$$

$$Q_{i,j} = \sum_{r=1}^{\infty}\sum_{s=1}^{\infty} r^j s^i P_r \mathrm{XP}_s \tag{A10}$$

Equation A10 is required for closure in the moment-based rate equations. Equation A10 can

be related to eq A9 through the following properties:

$$Q_0 = \frac{1}{2}\sum_{r=1}^{\infty}\sum_{s=1}^{r} P_{r-s}\mathrm{XP}_s - \frac{1}{2}\sum_{r=1}^{\infty} P_r\mathrm{XP}_0 = \frac{1}{2}\sum_{r=1}^{\infty}\sum_{s=1}^{\infty} P_r\mathrm{XP}_s = \frac{1}{2}Q_{0,0} \quad \text{(A11)}$$

$$Q_1 = \frac{1}{2}\sum_{r=1}^{\infty} r\sum_{s=1}^{r} P_{r-s}\mathrm{XP}_s - \frac{1}{2}\sum_{r=1}^{\infty} rP_r\mathrm{XP}_0 = \sum_{r=1}^{\infty}\sum_{s=1}^{\infty} rP_r\mathrm{XP}_s = Q_{1,0} \quad \text{(A12)}$$

$$Q_2 = \frac{1}{2}\sum_{r=1}^{\infty} r^2\sum_{s=1}^{r} P_{r-s}\mathrm{XP}_s - \frac{1}{2}\sum_{r=1}^{\infty} r^2P_r\mathrm{XP}_0 = \sum_{r=1}^{\infty}\sum_{s=1}^{\infty} r^2P_r\mathrm{XP}_s + \sum_{r=1}^{\infty}\sum_{s=1}^{\infty} rsP_r\mathrm{XP}_s = Q_{2,0} + Q_{1,1} \quad \text{(A13)}$$

The concentration-based rate equations that must be transformed are

$$\frac{\partial C_{\mathrm{XPr}}(t_1,t)\phi_{\mathrm{part}}(t_1,t)}{\partial t} = \sum_{s=1}^{\infty} k_{\mathrm{fra2}}P_r\mathrm{XP}_s(t_1,t) + k_{\mathrm{fra1}}P_r\mathrm{XP}_0(t_1,t) - k_{\mathrm{act1}}C_{\mathrm{XPr}}(t_1,t)P_0(t_1,t) - \sum_{s=1}^{\infty} k_{\mathrm{act2}}P_s(t_1,t)C_{\mathrm{XPr}}(t_1,t) \quad \text{(A14)}$$

$$\frac{\partial P_r\mathrm{XP}_s(t_1,t)}{\partial t} = k_{\mathrm{act2}}P_r(t_1,t)C_{\mathrm{XPs}}(t_1,t) + k_{\mathrm{act2}}P_s(t_1,t)C_{\mathrm{XPr}}(t_1,t) - 2k_{\mathrm{fra2}}P_r\mathrm{XP}_s(t_1,t) \quad \text{(A15)}$$

$$\frac{\partial P_r\mathrm{XP}_0(t_1,t)}{\partial t} = k_{\mathrm{act2}}P_r(t_1,t)C_{\mathrm{XR}}^{\mathrm{part}}(t) + k_{\mathrm{act1}}P_0(t_1,t)C_{\mathrm{XPr}}(t_1,t) - (k_{\mathrm{fra1}}+k_{\mathrm{fra2}})P_r\mathrm{XP}_0(t_1,t) \quad \text{(A16)}$$

$$\frac{\partial P_r(t_1,t)}{\partial t} = k_{\mathrm{p}}C_{\mathrm{mon}}^{\mathrm{part}}(t)P_{r-1}(t_1,t) + \sum_{s=1}^{\infty} k_{\mathrm{fra2}}P_r\mathrm{XP}_s(t_1,t) - \sum_{s=1}^{\infty} k_{\mathrm{act2}}P_r(t_1,t)C_{\mathrm{XPs}}(t_1,t) - k_{\mathrm{act2}}C_{\mathrm{XR}}^{\mathrm{part}}(t)P_r(t_1,t) + k_{\mathrm{fra2}}P_r\mathrm{XP}_0(t_1,t) - k_{\mathrm{p}}C_{\mathrm{mon}}^{\mathrm{part}}(t)P_r(t_1,t) \quad \text{(A17)}$$

where each species concentration is for a particle at time t that was previously initiated at time t_1. Using these concentration-based rate equations with the defined transformations (eqs A6–A10) gives the zero moment rate equations

$$\frac{\partial Y_0(t_1,t)}{\partial t} = 2k_{\mathrm{fra2}}Q_0(t_1,t) - k_{\mathrm{act2}}Y_0(t_1,t)G_0(t_1,t) + k_{\mathrm{p}}C_{\mathrm{mon}}^{\mathrm{part}}(t)P_0(t_1,t) - k_{\mathrm{act2}}C_{\mathrm{XR}}^{\mathrm{part}}(t)Y_0(t_1,t) + k_{\mathrm{fra2}}H_0(t_1,t) \quad \text{(A18)}$$

$$\frac{\partial G_0(t_1,t)\phi_{\mathrm{part}}(t_1,t)}{\partial t} = 2k_{\mathrm{fra2}}Q_0(t_1,t) + k_{\mathrm{fra1}}H_0(t_1,t) - k_{\mathrm{act1}}P_0(t_1,t)G_0(t_1,t) - k_{\mathrm{act2}}Y_0(t_1,t)G_0(t_1,t) \quad \text{(A19)}$$

$$\frac{\partial Q_0(t_1,t)}{\partial t} = k_{\mathrm{act2}}Y_0(t_1,t)\,G_0(t_1,t) - 2k_{\mathrm{fra2}}\,Q_0(t_1,t) \quad \text{(A20)}$$

$$\frac{\partial H_0(t_1,t)}{\partial t} = k_{\mathrm{act2}}\,C_{\mathrm{XR}}^{\mathrm{part}}(t)Y_0(t_1,t) + k_{\mathrm{act1}}\,P_0(t_1,t)\,G_0(t_1,t) - (k_{\mathrm{fra1}}+k_{\mathrm{fra2}})H_0(t_1,t) \quad \text{(A21)}$$

the first moment rate equations

$$\frac{\partial Y_1(t_1,t)}{\partial t} = k_P\,C_{\mathrm{mon}}^{\mathrm{part}}(t)\,Y_0(t_1,t) + k_{\mathrm{p}}\,C_{\mathrm{mon}}^{\mathrm{part}}(t)\,P_0(t_1,t) + k_{\mathrm{fra2}}\,Q_1(t_1,t) - k_{\mathrm{act2}}\,Y_1(t_1,t)\,G_0(t_1,t) - k_{\mathrm{act2}}\,C_{\mathrm{XR}}^{\mathrm{part}}(t)\,Y_1(t_1,t) + k_{\mathrm{fra2}}\,H_1(t_1,t) \quad \text{(A22)}$$

$$\frac{\partial G_1(t_1,t)\phi_{\text{part}}(t_1,t)}{\partial t} = k_{\text{fra2}}\, Q_1(t_1,t) + k_{\text{fra1}}\, H_1(t_1,t) - k_{\text{act1}}\, P_0(t_1,t)\, G_1(t_1,t) - k_{\text{act2}}\, G_1(t_1,t)\, Y_0(t_1,t) \quad \text{(A23)}$$

$$\frac{\partial Q_1(t_1,t)}{\partial t} = k_{\text{act2}}\, Y_1(t_1,t)\, G_0(t_1,t) + k_{\text{act2}}\, G_1(t_1,t)\, Y_0(t_1,t) - 2k_{\text{fra2}}\, Q_1(t_1,t) \quad \text{(A24)}$$

$$\frac{\partial H_1(t_1,t)}{\partial t} = k_{\text{act2}}\, C_{\text{XR}}^{\text{part}}(t)\, Y_1(t_1,t) + k_{\text{act1}}\, P_0(t_1,t) G_1(t_1,t) - (k_{\text{fra1}} + k_{\text{fra2}})\, H_1(t_1,t) \quad \text{(A25)}$$

and the second moment rate equations

$$\frac{\partial Y_2(t_1,t)}{\partial t} = k_P\, C_{\text{mon}}^{\text{part}}(t)(2Y_1(t_1,t) + Y_0(t_1,t)) + k_{\text{p}}\, C_{\text{mon}}^{\text{part}}(t)\, P_0(t_1,t) + k_{\text{fra2}}\, Q_{2,0}(t_1,t) - k_{\text{act2}} Y_2(t_1,t)\, G_0(t_1,t) - k_{\text{act2}}\, C_{\text{XR}}^{\text{part}}(t)\, Y_2(t_1,t) + k_{\text{fra2}}\, H_2(t_1,t) \quad \text{(A26)}$$

$$\frac{\partial G_2(t_1,t)\phi_{\text{part}}(t_1,t)}{\partial t} = k_{\text{fra2}}\, Q_{2,0}(t_1,t) + k_{\text{fra1}}\, H_2(t_1,t) - k_{\text{act1}}\, P_0(t_1,t)\, G_2(t_1,t) - k_{\text{act2}}\, G_2(t_1,t)\, Y_0(t_1,t) \quad \text{(A27)}$$

$$\frac{\partial Q_{2,0}(t_1,t)}{\partial t} = k_{\text{act2}}\, Y_2(t_1,t)\, G_0(t_1,t) + k_{\text{act2}}\, G_2(t_1,t)\, Y_0(t_1,t) - 2k_{\text{fra2}}\, Q_{2,0}(t_1,t) \quad \text{(A28)}$$

$$\frac{\partial Q_2(t_1,t)}{\partial t} = k_{\text{act2}}\, Y_2(t_1,t)\, G_0(t_1,t) + 2k_{\text{act2}}\, Y_1(t_1,t)\, G_1(t_1,t) + k_{\text{act2}}\, G_2(t_1,t)\, Y_0(t_1,t) - 2k_{\text{fra2}}\, Q_2(t_1,t) \quad \text{(A29)}$$

$$\frac{\partial H_2(t_1,t)}{\partial t} = k_{\text{act2}}\, C_{\text{XR}}^{\text{part}}(t)\, Y_2(t_1,t) + k_{\text{act1}}\, P_0(t_1,t)\, G_2(t_1,t) - (k_{\text{fra1}} + k_{\text{fra2}})\, H_2(t_1,t) \quad \text{(A30)}$$

The number of initiator radicals present is given by

$$\frac{\partial P_0(t_1,t)}{\partial t} = -k_{\text{p}}\, C_{\text{mon}}^{\text{part}}(t)\, P_0(t_1,t) + \sum_{r=1}^{\infty} k_{\text{fra1}}\, P_r \text{XP}_0(t_1,t) - \sum_{r=1}^{\infty} k_{\text{act1}}\, C_{X\,\text{Pr}}(t_1,t)\, P_0(t_1,t) \quad \text{(A31)}$$

This expression can also be transformed into an expression in terms of the defined moment equations (eqs A6–A10):

$$\frac{\partial P_0(t_1,t)}{\partial t} = -k_{\text{p}}\, C_{\text{mon}}^{\text{part}}(t)\, P_0(t_1,t) + k_{\text{fra1}}\, H_0(t_1,t) - k_{\text{act1}}\, P_0(t_1,t)\, G_0(t_1,t) \quad \text{(A32)}$$

These expressions are consistent with those used in the kinetic analysis because the zero moment rate equations (eqs A18–A21) are identical to eqs 2–6. With the 14 initial conditions at $t = t_1$

$$\begin{aligned} &Y_0 = 0, P_0 = \rho, Q_0 = 0, G_0 = 0, H_0 = 0 \\ &Y_1 = 0, Q_1 = 0, G_1 = 0, H_1 = 0 \\ &Y_2 = 0, Q_2 = 0, Q_{2,0} = 0, G_2 = 0, H_2 = 0 \end{aligned} \quad \text{(A33)}$$

and the monomer and RAFT profiles determined from the solution to the polymerization kinetics (eqs 10 and A5), eqs A18–A30 and A32 can be solved. The number-average molecular weight (M_{n}) and weight-average molecular weight (M_{w}) for the total population can then be determined from

$$M_n = \frac{\int_0^t \left(Y_1(t_1,t) + Q_1(t_1,t) + G_1(t_1,t)\phi_{\text{part}}(t_1,t) + H_1(t_1,t)\right)dt_1}{\int_0^t \left(Y_0(t_1,t) + Q_0(t_1,t) + G_0(t_1,t)\phi_{\text{part}}(t_1,t) + H_0(t_1,t)\right)dt_1} \tag{A34}$$

$$M_w = \frac{\int_0^t \left(Y_2(t_1,t) + Q_2(t_1,t) + G_2(t_1,t)\phi_{\text{part}}(t_1,t) + H_2(t_1,t)\right)dt_1}{\int_0^t \left(Y_1(t_1,t) + Q_1(t_1,t) + G_1(t_1,t)\phi_{\text{part}}(t_1,t) + H_1(t_1,t)\right)dt_1} \tag{A35}$$

REFERENCES AND NOTES

1. Barner-Kowollik, C.; Davis, T. P.; Heuts, J. P. A.; Stenzel, M. H.; Vana, P.; Whittaker, M. J Polym Sci Part A: Polym Chem 2003, 41, 365–375.
2. Chiefari, J.; Chong, Y. K.; Ercole, F.; Krstina, J.; Jeffery, J.; Le, T. P. T.; Mayadunne, R. T. A.; Meijs, G. F.; Moad, C. L.; Moad, G.; Rizzardo, E.; Thang, S. H. Macromolecules 1998, 31, 5559–5562.
3. Prescott, S. W.; Ballard, M. J.; Rizzardo, E.; Gilbert, R. G. Aust J Chem 2002, 55, 415–424.
4. Ferguson, C. J.; Hughes, R. J.; Nguyen, D.; Pham, B. T. T.; Gilbert, R. G.; Serelis, A. K.; Such, C. H.; Hawkett, B. S. Macromolecules 2005, 38, 2191–2204.
5. de Brouwer, H.; Tsavalas, J. G.; Schork, F. J.; Monteiro, M. J. Macromolecules 2000, 33, 9239–9246.
6. Liu, S.; Hermanson, K. D.; Kaler, E. W. Macromolecules 2006, 39, 4345–4350.
7. Barner-Kowollik, C.; Quinn, J. F.; Nguyen, T. L. U.; Heuts, J. P. A.; Davis, T. P. Macromolecules 2001, 34, 7849–7857.
8. Wang, A. R.; Zhu, S. P. J Polym Sci Part A: Polym Chem 2003, 41, 1553–1566.
9. Johnston-Hall, G.; Theis, A.; Monteiro, M. J.; Davis, T. P.; Stenzel, M. H.; Barner-Kowollik, C. Macromol Chem Phys 2005, 206, 2047–2053.
10. Monteiro, M. J. J Polym Sci Part A: Polym Chem 2005, 43, 3189–3204.
11. Zhang, M.; Ray, W. H. Ind Eng Chem Res 2001, 40, 4336–4352.
12. Luo, Y. W.; Wang, R.; Yang, L.; Yu, B.; Li, B. G.; Zhu, S. P. Macromolecules 2006, 39, 1328–1337.
13. Monteiro, M. J.; Hodgson, M.; De Brouwer, H. J Polym Sci Part A: Polym Chem 2000, 38, 3864–3874.
14. Luo, Y. W.; Yu, B. Polym Plast Technol Eng 2004, 43, 1299–1321.
15. Smulders, W.; Gilbert, R. G.; Monteiro, M. J. Macromolecules 2003, 36, 4309–4318.
16. Prescott, S. W.; Ballard, M. J.; Rizzardo, E.; Gilbert, R. G. Macromolecules 2005, 38, 4901–4912.
17. Barner-Kowollik, C.; Coote, M. L.; Davis, T. P.; Radom, L.; Vana, P. J Polym Sci Part A: Polym Chem 2003, 41, 2828–2832.
18. Monteiro, M. J.; de Brouwer, H. Macromolecules 2001, 34, 349–352.
19. Wang, A. R.; Zhu, S. P.; Kwak, Y. W.; Goto, A.; Fukuda, T.; Monteiro, M. S. J Polym Sci Part A: Polym Chem 2003, 41, 2833–2839.
20. Kwak, Y.; Goto, A.; Tsujii, Y.; Murata, Y.; Komatsu, K.; Fukuda, T. Macromolecules 2002, 35, 3026–3029.
21. Coote, M. L.; Radom, L. J Am Chem Soc 2003, 125, 1490–1491.
22. Barner-Kowollik, C.; Quinn, J. F.; Morsley, D. R.; Davis, T. P. J Polym Sci Part A: Polym Chem 2001, 39, 1353–1365.
23. Calitz, F. M.; McLeary, J. B.; McKenzie, J. M.; Tonge, M. P.; Klumperman, B.; Sanderson, R. D. Macromolecules 2003, 36, 9687–9690.
24. Kwak, Y.; Goto, A.; Komatsu, K.; Sugiura, Y.; Fukuda, T. Macromolecules 2004, 37, 4434–4440.
25. Venkatesh, R.; Staal, B. B. P.; Klumperman, B.; Monteiro, M. J. Macromolecules 2004, 37, 7906–7917.
26. Ah Toy, A.; Vana, P.; Davis, T. P.; Barner-Kowollik, C. Macromolecules 2004, 37, 744–751.
27. Drache, M.; Schmidt-Naake, G.; Buback, M.; Vana, P. Polymer 2005, 46, 8483–8493.
28. Morgan, J. D.; Lusvardi, K. M.; Kaler, E. W. Macromolecules 1997, 30, 1897–1905.
29. Guo, J. S.; Sudol, E. D.; Vanderhoff, J. W.; El-Aasser, M. S. J Polym Sci Part A: Polym Chem 1992, 30, 703–712.
30. Guo, J. S.; Sudol, E. D.; Vanderhoff, J. W.; El-Aasser, M. S. J Polym Sci Part A: Polym Chem 1992, 30, 691–702.
31. Candau, F. In Polymerization in Organized Media; Paleos, C. M., Ed.; Gordon & Breach: Philadelphia, 1992; pp 215–282.
32. Full, A. P.; Kaler, E. W.; Arellano, J.; Puig, J. E. Macromolecules 1996, 29, 2764–2775.
33. Co, C. C.; de Vries, R.; Kaler, E. W. Macromolecules 2001, 34, 3224–3232.
34. Co, C. C.; Cotts, P.; Burauer, S.; de Vries, R.; Kaler, E. W. Macromolecules 2001, 34, 3245–3254.
35. de Vries, R.; Co, C. C.; Kaler, E. W. Macromolecules 2001, 34, 3233–3244.

36. Co, C. C.; Kaler, E. W. Macromolecules 1998, 31, 3203–3210.
37. Vana, P.; Davis, T. P.; Barner-Kowollik, C. Macromol Theory Simul 2002, 11, 823–835.
38. Perrier, S.; Barner-Kowollik, C.; Quinn, J. F.; Vana, P.; Davis, T. P. Macromolecules 2002, 35, 8300–8306.
39. Fischer, H.; Radom, L. Angew Chem Int Ed 2001, 40, 1340–1371.
40. Polymer Handbook; Brandrup, J.; Immergut, E. H. Eds.; Wiley: New York, 1989.
41. Beuermann, S.; Buback, M.; Davis, T. P.; Gilbert, R. G.; Hutchinson, R. A.; Olaj, O. F.; Russell, G. T.; Schweer, J.; van Herk, A. M. Macromol Chem Phys 1997, 198, 1545–1560.
42. Petzold, L. R. DDASSL code build 910624; Lawrence Livermore National Laboratory: Livermore, CA, 1991.
43. Chong, Y. K.; Krstina, J.; Le, T. P. T.; Moad, G.; Postma, A.; Rizzardo, E.; Thang, S. H. Macromolecules 2003, 36, 2256–2272.
44. Goto, A.; Sato, K.; Tsujii, Y.; Fukuda, T.; Moad, G.; Rizzardo, E.; Thang, S. H. Macromolecules 2001, 34, 402–408.
45. Dotson, N. A.; Galvan, R.; Laurence, R. L.; Tirrell, M. Polymerization Process Modeling; VCH: New York, 1996; p 45.